International Journal of Mining and Geo-Engineering

IJMGE

IJMGE 51-1 (2017) 9–22

DOI: 10.22059/ijmge.2016.218483.594634

Combined application of computational fluid dynamics (CFD) and design of experiments (DOE) to hydrodynamic simulation of a coal classifier

Hamid Khoshdast [a], Vahideh Shojaei [a,*], Hami Khoshdast [b]

[a] *Department of Mining Engineering, Higher Education Complex of Zarand, Zarand, Iran*

[b] *Mechanical Engineering Division, INVENTIVE® Mineral Processing Research Center, Zarand, Iran*

Article History:

Received 23 October 2016,
Revised 27 December 2016,
Accepted 30 December 2016.

ABSTRACT

Combining two methods of computational fluid dynamics (CFD) and design of experiments (DOE) was proposed in modeling to simultaneously benefit from the advantages of both modeling methods. The presented method was validated using a coal hydraulic classifier in an industrial scale. The effects of operating parameters, including feed flow rate, solid content and baffle length, were evaluated based on the classifier overflow velocity and cut-size as the process responses. The evaluation sequence was as follows: the variation levels of parameters was first evaluated using industrial measurement, and then a suitable experimental design was carried out and the DOE matrix was translated to CFD input. Afterwards, the overflow velocity values were predicted by CFD, and the cut-size values were determined using industrial and CFD results. The overflow velocity and cut-size values were statistically analyzed to develop the prediction models for DOE responses; and finally, the main interaction effects were interpreted with respect to DOE and CFD results. Statistical effect plots along with CFD fluid flow patterns showed the effects of type and magnitude of operating parameters on the classifier performance, and visualized the mechanism by which those effects occurred. The suggested modeling method seems to be a useful approach for better understanding the real operational phenomena within the fluid-base separation devices. Furthermore, the individual interaction effects can also be identified and used for interpretation of responses in nonlinear processes.

Keywords : *modeling, hydrodynamic simulation, experimental design, hydraulic classifier, industrial application*

1. Introduction

Hydraulic classifiers are widely applied in mineral processing industries for washing and/or sorting the particulate feeds. Common applications of hydraulic classifiers include fine coal classification, dewatering of coal tailings prior to centrifugation [1], clay removal from siliceous sands [2, 3], purification of cement materials [4], particle size control in closed grinding circuits [4, 5], fine particles control in iron pellet washing, the removal of silica from iron ores [5]. Hydraulic classifiers actually consist of a sorting chamber in which a moving fluid, commonly water, divides an input stream of particles with a wide size distribution into two fine overflow and coarse underflow products. The overflow stream is generally considered as the final treated product directed to the downstream processing units. The accepted representative measure for evaluation of a classifier performance is the cut-size value (d_{50}) that is the size giving particles an equal chance to join overflow or underflow streams [6].

Since hydraulic classifiers use the governing rules of fluid flow in a predefined geometry, the computational fluid dynamics (CFD) method can be used for simulation of hydrodynamic response of classifier to the changes in operating parameters. CFD uses numerical methods to solve the fundamental nonlinear differential equations to describe the fluid flow pattern and to predict the flow velocity in each region within the classifier chamber wherein flow occurs. CFD helps engineers to evaluate the effects of operating parameters on the system performance with less time, expense, and also disruption that is required to make actual physical changes to the existing system. CFD also uses a very compelling non-intrusive virtual modeling technique with powerful visualization capabilities, and the obtained information reveals what modification satisfies the design criteria. Additionally, the selected fundamental equations for CFD modeling process can be validated by experimental data to enhance the reliability of simulation results [7]. Computational fluid dynamics has been successfully used to model the effects of operating factors on the operational performance of different type of classifiers. For example, Bhaskar et al. [8, 9] simulated the performance of hydrocyclone using different types of turbulence models and evaluated the effect of multiple operating parameters, including spigot opening and inlet pressure, on vertical velocity of water within the cyclone chamber. Narasimha et al. [10] used a multiphase CFD model with sub-modules for the air-core turbulence and particle classification with a suitable slurry viscosity model to simulate the performance of hydrocyclones. They showed that the overall classification curve predicted close to the experimental data. Swain and Mohanty [11] simulated hydrocyclones in solid-liquid state using an Eulerian–Eulerian CFD approach. They indicated that under two-phase simulation conditions, different turbulence models showed slight variation in prediction of the velocity profile and the separation efficiency. The maximum deviation between the two models was observed near the wall where the stress was maximum for larger particles. Recently, Kępa [12] applied CFD method to improve the efficiency of a large-diameter cyclone. He showed that the applied model correctly reflected the flow through the device and facilitated the estimation of the separation efficiency. Safa and Goharrizi [13] optimized the performance of an industrial hydrocyclone by applying a three-dimensional computational fluid dynamics simulation together

* Corresponding author. Tel.: (+98)9132953766; Fax: (+98)3431242040. *E-mail address:* v.shojaei@uk.ac.ir (V. Shojaei).

with experimental field measurements. They investigated the effect of inlet solid percentage, pulp inlet velocity, rod inserted in the middle of the hydrocyclone, and apex diameter on hydrocyclone performance. Johansson and Evertsson [14, 15] used computational fluid dynamics to improve the understanding of the influence of the geometric design of the air classifiers on the cut size and the resulting particle size distribution. Simulations were performed with a CFD model using an Euler–Lagrange approach. Their simulation results showed that the classification results are affected by air flow velocity, particle shape, particle size, the geometry of the air classifier, and the turbulence in air flow. Jarkani et al. [16] modeled the effects of structural and dimensional manipulations on hydrodynamic behaviour of a bench vertical current classifier. They confirmed the goodness of CFD application in optimized design of vertical current classifiers. Apart from advantages of CFD method, engineers can only simulate the process response through one factor at a time strategy while holding other parameters at a constant level; thus, interaction effects between dependent variables are disregarded. A more effective method which has recently attracted the attention of engineers is to apply a systematic approach to experimentation so that one can simultaneously consider all factors. This approach is called design of experiments (DOE) that provides useful information about the interaction of operating variables and the way the total system works by using statistical analyses [13].

There are different parameters affecting the performance of hydraulic classifiers which can be categorized into operating and mechanical factors. Operating parameters include those related to the input feed characteristics and mechanical factors are the design and dimensional aspects of classifier. The effects of these parameters on classifier performance and the products selectivity and quality have been investigated by several researchers. Table 1 summarizes the studied parameters reported in literature.

Table 1. Parameters affecting the performance of hydraulic classifiers

Type of parameter	Parameter [Reference]
Operating parameters	Feed pulp density [17, 19, 20, 29], Feed flow rate [18, 22, 31], Particle size [18-20, 22, 25], Particle density [20, 22, 25]
Mechanical factors	Capacity [17], Fluidization rate [17, 22, 27, 29-31], Rotor speed [18, 24], Rotor aspects ratio [18, 24], Sorting chamber aspect ratio [21, 25, 26], Product discharge diameter [21] and curvature [32], Baffle aspect ratio [16, 21, 23, 32] and angle [16, 23, 32], Teeter bed hole diameter [26, 28] and pattern [28]

2. Stages in the Modeling Process

The modeling was carried out based on the following sequence, as schematically is shown in Fig. 1:

Studies started with collecting metallurgical data from a coal hydraulic classifier at Zarand Coal Washing Plant (Zarand, Iran) to determine variation ranges for operating parameters,

An experimental design was constructed for assessment of the effects of operating variables on process responses; overflow velocity, flow rate and cut-size were considered as process responses,

The statistical experimental design was converted into the computational fluid dynamics modeling input,

The CFD model was developed and validated by using a series of batch experiments,

The overflow velocity value for each translated DOE run was predicted by CFD model and then, results were put in original statistical DOE,

Modeling results were statistically analyzed using analyses of variance (ANOVA) methodology,

A statistical model was then developed for evaluation of how operating variables affect the considered process responses,

Finally, the effects of operating parameters on product cut-size were interpreted using statistical and CFD modeling results.

2.1. Industrial Investigations

Fig. 2 shows the schematic illustration of studied hydraulic classifier at Zarand Coal Washing Plant, Zarand, Iran. As seen in Fig. 2, classifier is fed by different pulp lines and yields an underflow tailings product and an overflow stream as the final classification product which is further processed in flotation circuit. Cut-size of overflow product is a key factor for evaluation of classifier performance. Thus, the effects of operating parameters on cut-size are required to be investigated continuously by quality control division. In this study, feed pulp flow rate and solid content were first considered as the experimental variables. These parameters are those which can be easily manipulated by technical engineers in the plant. The effect of operating variables was evaluated using an experimental design described in the next section. The experimental data were measured using the samples that were collected following an 8-month sampling program; therefore, 140 representative samples were collected from feed and product streams. For preparing each representative sample, 5 sub-samples of volume 20 liters were collected in each operating shift and then mixed, dried and divided to obtain appropriate weight of the sample (about 500 g) for particle size analysis. Each sample was collected using a 30-lit bucket. Other parameters including pulp flow rate and solids content were also measured during the sample collection period. Feed flow rate was calculated by dividing the volume of each incremental sample by the time taken to fill the bucket. Solids content of each representative sample was determined by weighing the samples before and after drying. Actual cut size values were also determined by plotting the partition coefficient curve for each sample, i.e. each particle size fraction in feed were transferred to the underflow stream.

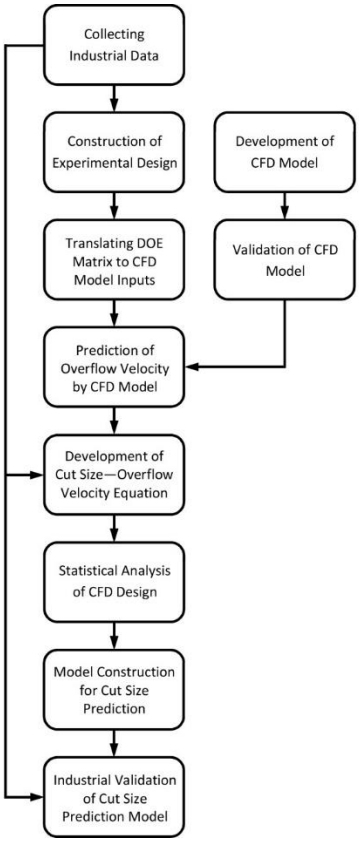

Fig. 1. Stages considered for development of the proposed modeling approach.

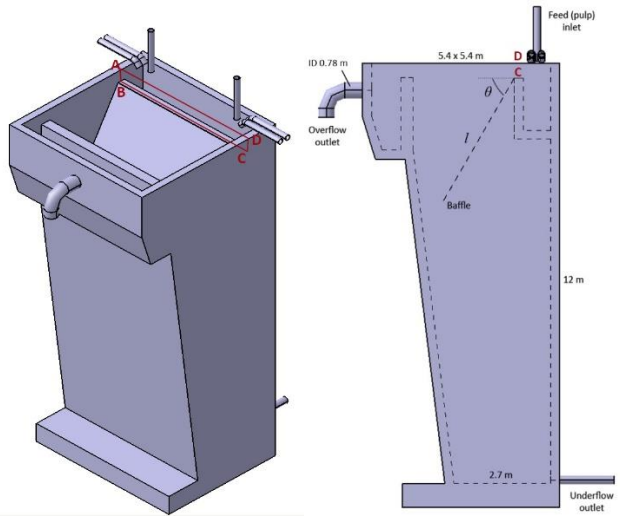

Fig. 2. 3D view and dimensional drawing of the coal hydraulic classifier used for simulations.

2.2. Construction of experimental design

Different types of experimental designs have been developed by statisticians. The choice of appropriate design depends on the objectives of investigations and the number of parameters to be investigated. Since the main objective of this study was to investigate the effects of operating parameters on hydrodynamic response of classifier, full factorial design was selected. Full factorial is a suitable designing technique which is commonly used for process analysis and modeling [38, 39]. This statistical design helps researchers to introduce mathematical equations that describe the way the studied variables affect the target response(s). Additionally, full factorial design allows one to estimate the interaction effects and the nonlinear relations between the variables and existing response [40].

A full factorial design requires at least three levels for each variable to estimate the coefficients of the nonlinear terms in the prediction model. The levels of interest for each operating variable were selected based on the variation ranges of input and output variables measured during industrial investigations in the plant. As shown in Fig. 2, the classifier is equipped with a removable baffle plate of 3.9 m in length, to moderate turbulence condition inside the classifier chamber. As technical engineers requested, the effect of baffle presence or absence on cut-size was also considered in experimental design. Therefore, a theoretical mid-length of 1.95 m was also included in the factorial design to evaluate the potential nonlinear effect of baffle length. However, it should be noted that the classifier was equipped with original baffle plate with a length of 3.9 m during industrial sampling program. Table 2 presents the considered ranges for studied variables. The experimental design matrix shown in Table 3 consists of a three-level full factorial design with 27 experimental points ($3^3 = 27$).

Table 2. Independent variables and their levels for full factorial design.

Coded Symbol	Variables	Units	Variable level		
			-1	0	+1
A	Feed flowrate (*Q*)	m^3/s	0.05	1.55	3.05
B	Solid content (*X*)	%	5	15	25
C	Baffle length (*L*)	m	0	1.95	3.9

2.3. Computational Fluid Dynamic Modeling

2.3.1. The model theory

Incompressible Navier-Stokes equation in combination with a turbulent flow model is commonly applied for simulation of flow patterns in water-base separators. To predict the fluid flow pattern in hydraulic classifier studied in this paper, the governing equation consists of the continuity and momentum balance equations for the liquid phase, as follows [16]:

$$\nabla \cdot \rho v = 0 \tag{1}$$

$$\nabla \cdot \rho \vec{v}\vec{v} = -\nabla p + \nabla . \vec{\tau} + \rho \vec{g} \tag{2}$$

where ρ is the fluid density, g denotes the gravity, v represents the velocity of fluid, and p is the static pressure. The stress tensor τ can be calculated as follows:

$$\vec{\tau} = \mu_{effective}\left[\nabla v - \frac{2}{3}\nabla \cdot \rho \vec{v}^2\right] \tag{3}$$

$$\mu_{effective} = \mu + \mu_t \tag{4}$$

where μ and μeffective are dynamic and effective viscosity, respectively [8]. The momentum equation can be solved using a turbulent flow (TF) model. The standard k–ε dispersed turbulence model is a TF model commonly used for engineering purposes. Variables k and ε indicate turbulent kinetic energy and turbulent dissipation rate, respectively. The k–ε model is solved using the following equations:

$$\frac{\partial}{\partial t}(\rho k) + \frac{\partial}{\partial X_i}(\rho k u_i) = \frac{\partial}{\partial X_j}\left[\left(\mu + \frac{\mu_i}{\sigma_k}\right)\frac{\partial k}{\partial X_j}\right] + G_k - \rho\varepsilon \tag{5}$$

$$\frac{\partial}{\partial t}(\rho \varepsilon) + \frac{\partial}{\partial X_i}(\rho \varepsilon u_i) = \frac{\partial}{\partial X_j}\left[\left(\mu + \frac{\mu_i}{\sigma_\varepsilon}\right)\frac{\partial k}{\partial X_j}\right] + C_{1\varepsilon}\frac{\varepsilon}{k}G_k - C_{2\varepsilon}\rho\frac{\varepsilon^2}{k} \tag{6}$$

where Gk is the kinetic energy due to velocity gradient and μt is the viscosity of turbulent flow. These parameters can be calculated using the following equations:

$$G_k = \rho \overline{u_i' u_j'}\frac{\partial u_j}{\partial x_i} \tag{7}$$

$$\mu_t = \rho C_\eta \frac{k^2}{\varepsilon} \tag{8}$$

where *u'* is the velocity vector and $C_{1\varepsilon}$, $C_{2\varepsilon}$, σ_k, σ_ε and C_η are constants [16].

2.3.2. Industrial scale modeling

This simulation used the steady state pressure based implicit formulation of Fluent 6.3 software [41] which employs the finite volume method and the 3D physical meshing of the classifier that was constructed in pre-processor Gambit 2.3. The whole computational domain was divided into structured hexahedron grids. A "velocity inlet" boundary condition was used at the classifier inlet and outlets. The initial and boundary conditions were set on the basis of experimental data: inlet pulp velocity of 3 m/s, pulp density of 1099 kg/m^3 (15% solid content), and atmospheric pressure. As seen in Fig. 2, the classifier is fed by different pulp lines; therefore, the discharge gate of the classifier feed box (ABCD section) was considered as feed inlet to simplify the graphical construction of meshing design. In order to approximate more accurate results, the residual convergence and iteration values were fixed at $1x10^{-5}$ and 30,000, respectively [41, 42].

2.3.3. Validation of model

The model validation was carried out through the experimental data that where gathered based on a set of batch tests at laboratory using a bench scale hydraulic classifier (Fig. 3). Pulp flowrate (*Q*) and density (*D*) were selected as operating parameters (Table 4). Afterwards, pulp velocity in overflow discharge gate in the used hydraulic classifier was predicted and plotted against the predicted values.

3. Results and Discussion

3.1. Validation of CFD model

Pulp velocity values in overflow outlet as the response of experimental design are listed in Table 4. To assess the accuracy of CFD model, the determination coefficient (R^2) was calculated as follows [43]:

$$R^2 = 1 - \frac{SS_{res}}{SS_{tot}}$$

where SS_{res} and SS_{tot} are residual and total sum of squares, respectively,

$$SS_{res} = \sum_i (v_{exp,i} - v_{model,i})^2$$

$$SS_{tot} = \sum_i (v_{exp,i} - \bar{v}_{exp,i})^2$$

As shown in Fig. 5, the predicted values are in good agreement with the experimental measurements. This confirms the accuracy of the chosen model.

Table 3. Full factorial design consisted of experiments for the study of operating parameters with experimental and predicted results.

Run	Feed flowrate (Q) (m^3/s)	Solid content (X) (%)	Baffle length (L) (m)	Overflow responses					
				Velocity (m/s)		Flow rate (m^3/s)		Cut-size (μm)	
				Actual[1]	Pred.[2]	Actual[3]	Pred.[4]	Actual[5]	Pred.[6]
1	0.05	5	0	0.008342	0.021348	0.003984	0.010196	37.4251	38.0881
2	0.05	15	0	0.008388	0.007354	0.004006	0.003512	37.5058	37.7285
3	0.05	25	0	0.008418	0.003550	0.004021	0.001700	37.5583	36.6725
4	0.05	5	1.95	0.008601	0.010190	0.004108	0.004870	37.8762	35.7813
5	0.05	15	1.95	0.008627	0.064815	0.004120	0.030955	37.9210	43.8628
6	0.05	25	1.95	0.008654	0.028740	0.004133	0.013730	37.9675	34.1206
7	0.05	5	3.9	0.009974	0.015762	0.004763	0.007528	40.1397	41.5716
8	0.05	15	3.9	0.010004	0.045150	0.004778	0.021560	40.1869	34.0223
9	0.05	25	3.9	0.010050	0.059416	0.004800	0.028377	40.2592	44.9918
10	1.55	5	0	0.456209	0.511862	0.217883	0.244462	179.5739	186.4262
11	1.55	15	0	0.517756	0.482656	0.247277	0.230514	188.7046	184.0512
12	1.55	25	0	0.540632	0.520079	0.258203	0.248387	191.9292	189.7303
13	1.55	5	1.95	0.486274	0.468455	0.232242	0.223732	184.1219	182.1080
14	1.55	15	1.95	0.497385	0.528252	0.237548	0.252290	185.7593	188.1741
15	1.55	25	1.95	0.496078	0.483030	0.236924	0.230692	185.5679	185.1670
16	1.55	5	3.9	0.590958	0.553124	0.282238	0.264169	198.7421	193.9037
17	1.55	15	3.9	0.472767	0.477000	0.225791	0.227813	182.1004	184.3390
18	1.55	25	3.9	0.596296	0.629897	0.284787	0.300835	199.4437	202.0436
19	3.05	5	0	0.845316	0.776657	0.403718	0.370927	228.6734	221.1581
20	3.05	15	0	0.800000	0.836133	0.382075	0.399332	223.7885	228.2191
21	3.05	25	0	0.874727	0.907253	0.417765	0.433299	231.7590	234.8437
22	3.05	5	1.95	0.759226	0.795839	0.362602	0.380088	219.2473	223.3561
23	3.05	15	1.95	1.031372	0.944318	0.492577	0.451000	247.2147	238.8581
24	3.05	25	1.95	0.882352	0.932793	0.421406	0.445496	232.5487	236.7965
25	3.05	5	3.9	0.895205	0.927251	0.427545	0.442850	233.8704	237.2769
26	3.05	15	3.9	0.888888	0.939809	0.424528	0.448848	233.2222	237.1482
27	3.05	25	3.9	1.209370	1.126403	0.577588	0.537964	263.1308	255.7983

[1] Calculated by CFD model
[2] Calculated by Eq. (18)
[3] Calculated by Eq. (16)
[4] Calculated by Eq. (19)
[5] Calculated by Eq. (21)
[6] Calculated by Eq. (22)

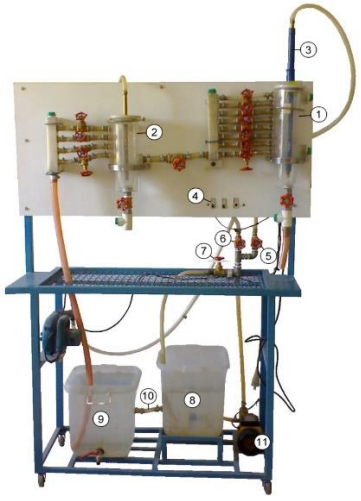

Fig. 3. Bench scale hydraulic classifier used in validation study: (1) classification vessel, (2) overflow vessel, (3) pulp inlet, (4) control fuse, (5-7) pulp control valves, (8-10) pulp tanks and connections, and (11) hydraulic pump.

Table 4. Experimental design matrix and results for validation study

run	Pulp density, D (kg/m^3)	Pulp flowrate, Q (lit/min)	Overflow velocity (m/s)	
			Actual	Predicted
1	1210	14	0.632	0.64
2	1210	10	0.3491	0.352
3	1210	5	0.177	0.19
4	1094	14	0.6095	0.59
5	1094	10	0.328	0.319
6	1094	5	0.137	0.113
7	1045	14	0.58	0.5845
8	1045	10	0.311	0.333
9	1045	5	0.1038	0.13

3.2. Statistical analysis of CFD modeling results

Since particle size is not directly employed as an operating variable, the feed flowrate and solid content were converted into different states as CFD modeling inputs. Feed flowrate can be easily converted to feed velocity as follows:

$$V_f = \frac{Q}{A_f} \quad (12)$$

where V_f is the feed velocity (m/s), Q represents the feed flowrate (m^3/s) and A_f denotes the cross sectional area of feed inlet (m^2). Solids content directly affects the pulp rheology, therefore, it can be stated as two parameters of feed density and viscosity, as well. Solid content can be calculated on the basis of density value of the feed components, i.e. particles and water, using Eq. (13) [6]:

$$X = \frac{S(D-W)}{D(S-W)} \quad (13)$$

where S, D and W are density values for solid phase, pulp and water, respectively. In this study, particles and water densities were 2500 kg/m^3 and 1000 kg/m^3, respectively. Pulp viscosity can be calculated using Arrhenius equation as follows [44]:

$$\mu_p = \mu_w \exp(k.\varphi) \quad (14)$$

where μ_p is the pulp viscosity, μ_w is the water viscosity (0.001 kg/ms at ambient temperature), k represents a constant value (0.338 in this study), and φ stands for the volumetric solid content in pulp. φ per unit volume of pulp is calculated as follows [6]:

$$\varphi = \frac{XD}{100S} \quad (15)$$

Now, the experimental matrix given in Table 3 can be converted into an easier design shown in Table 5. Parameters given in Table 5 are used as input variables for CFD modeling process. CFD modeling results are shown in Table 5.

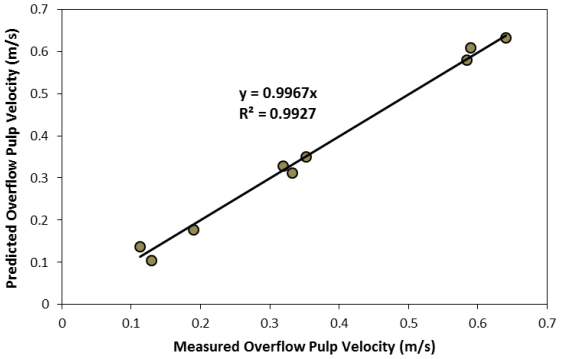

Fig. 4. Comparison between experimental data and simulation results during validation study.

Table 5. Experimental design with variables translated to CFD modeling language

Run	V_f (m/s)	D (Kg/m^3)	μ_p (10^{-3} Kg/ms)	L (m)	Overflow velocity as response, V_o (m/s)
1	0.009758	1.031	1.007	0	0.008342
2	0.009758	1.099	1.022	0	0.008388
3	0.009758	1.177	1.041	0	0.008418
4	0.009758	1.031	1.007	1.95	0.008601
5	0.009758	1.099	1.022	1.95	0.008627
6	0.009758	1.177	1.041	1.95	0.008654
7	0.009758	1.031	1.007	3.9	0.009974
8	0.009758	1.099	1.022	3.9	0.010004
9	0.009758	1.177	1.041	3.9	0.010050
10	0.3026	1.031	1.007	0	0.456209
11	0.3026	1.099	1.022	0	0.517756
12	0.3026	1.177	1.041	0	0.540632
13	0.3026	1.031	1.007	1.95	0.486274
14	0.3026	1.099	1.022	1.95	0.497385
15	0.3026	1.177	1.041	1.95	0.496078
16	0.3026	1.031	1.007	3.9	0.590958
17	0.3026	1.099	1.022	3.9	0.472767
18	0.3026	1.177	1.041	3.9	0.596296
19	0.5954	1.031	1.007	0	0.845316
20	0.5954	1.099	1.022	0	0.800000
21	0.5954	1.177	1.041	0	0.874727
22	0.5954	1.031	1.007	1.95	0.759226
23	0.5954	1.099	1.022	1.95	1.031372
24	0.5954	1.177	1.041	1.95	0.882352
25	0.5954	1.031	1.007	3.9	0.895205
26	0.5954	1.099	1.022	3.9	0.888888
27	0.5954	1.177	1.041	3.9	1.209370

It should be noted that the experimental matrix in Table 5 cannot be used as an input to analysis the software; because it is not actually a statistically designed experimental program. Therefore, experimental design shown in Table 3 is used for interpretation. According to the design matrix given in Table 3, 27 tests were conducted following the sequence defined by Design-Expert Software v.7.1.5 (DX7).

Pulp velocity in overflow outlet can be easily converted to pulp flowrate by using Eq. (16):

$$Q_o = V_o \times A_o \quad (16)$$

where Q_o is the overflow rate (m^3/s), V_o is the overflow velocity as predicted by CFD modeling (m/s) and A_o is the cross sectional area of overflow outlet (0.48 m^2). Pulp flowrate values calculated by Eq. (16) are listed in Table 3. Then, two responses were evaluated, i.e., the overflow velocity and flowrate. A nonlinear equation was developed to predict the responses as a function of independent variables [40, 45, 46]. In general, the experimental data obtained from the designed experiment is

analyzed by nonlinear regression procedure using the following multi-variable equation:

$$y = b_0 + \sum b_i x_i + \sum b_{ij} x_i x_j + \varepsilon \quad (17)$$

where y is the predicted response, b_0 represents the constant coefficient, b_i is the linear coefficients, b_{ij} denotes the nonlinear coefficients, x_i and x_j are coded values of the independent process variables, and ε is the residual error. The values of the coefficients were calculated by using DX7 software. The best fitted model equation was obtained for overflow pulp velocity as follows:

$$\begin{aligned}\text{Overflow velocity} = {} & 0.479 - 0.469Q_1 + 0.039Q_2 \\ & - 0.027X_1 - 0.008X_2 - 0.027L_1 - 0.014L_2 \\ & + 0.027Q_1X_1 + 0.021Q_2X_1 + 0.008Q_1X_2 - 0.013Q_2X_2 \\ & + 0.027Q_1L_1 + 0.015Q_2L_1 + 0.014Q_1L_2 - 0.009Q_2L_2 \\ & + 0.013X_1L_1 - 0.001X_2L_1 - 0.019X_1L_2 + 0.056X_2L_2\end{aligned} \quad (18)$$

and for overflow rate in below:

$$\begin{aligned}\text{Overflow rate} = {} & 0.229 - 0.224Q_1 + 0.018Q_2 \\ & - 0.013X_1 - 0.004X_2 - 0.013L_1 - 0.007L_2 \\ & + 0.013Q_1X_1 + 0.01Q_2X_1 + 0.004Q_1X_2 \\ & - 0.006Q_2X_2 + 0.013Q_1L_1 + 0.007Q_2L_1 \\ & + 0.007Q_1L_2 - 0.005Q_2L_2 + 0.006X_1L_1 \\ & - 0.001X_2L_1 - 0.009X_1L_2 + 0.027X_2L_2\end{aligned} \quad (19)$$

where indices 1 and 2 show the lower and upper domains of levels respectively, i.e. values which are smaller and larger than mid-level of each variable, respectively. Model Eqs. (18) and (19) were used to evaluate the influence of process variables on the overflow velocity and flowrate. Analysis of Variance (ANOVA) was performed to assess the models significance. ANOVA results (Tables 6 and 7) of the regression models suggested that both models were highly significant, as was evident from Fisher's F-test (F model = 151.68) with a very low probability value (p model < 0.0001). Significance of each variable was also determined by p-values, as listed in Tables 6 and 7. "Prob > F" values of less than 0.05 (for confidence interval of 95%) indicate that the model terms are significant. As seen in Table 6, all single and multiple effects were significant terms for the overflow velocity model. Similar results were expected for overflow rate model since this response is actually the overflow velocity multiplied by a constant value, i.e. cross sectional area of overflow outlet. Table 7 shows that all single and multiple effects were also significant model terms for overflow rate response.

Normal probability plot of the residuals is a useful tool to be used for detecting the normal distribution, the independency of model errors, and the homogeneity of the variance error [47]. Normal probability of the residuals of overflow velocity presented in Fig. 5 showed almost no serious violation of the assumptions underlying the analyses that confirmed the normality assumptions and independency of the residuals. All of above considerations confirmed the adequacy of the developed relationship. A high value of R^2 (98.73%) indicates high correlation between the measured and predicted values of the response. Moreover, a closely high value of the adjusted correlation coefficient (Adj R^2 = 98.08%) also shows a high significance for the model. On the other hand, total variation of about 98% for the overflow velocity was attributed to the independent variables, and only about 2% of total variation could not be explained by developed model.

Table 6. Analysis of variance (ANOVA) of the full factorial model to predict overflow velocity

Source	Sum of Squares	df	Mean Square	F Value	p-value Prob > F	
Model	7.574336	18	0.420796	151.6795	< 0.0001	**significant**
Feed flowrate (Q)	7.339871	2	3.669936	1322.858	< 0.0001	
Solid content (X)	0.037387	2	0.018694	6.738302	0.0033	
Baffle length (L)	0.048749	2	0.024374	8.78594	0.0008	
QX	0.042632	4	0.010658	3.841728	0.0109	
QL	0.041283	4	0.010321	3.720199	0.0126	
XL	0.064414	4	0.016104	5.80468	0.0011	
Residual	0.097099	35	0.002774			
Lack of Fit	0.097099	8	0.012137			
Pure Error	0	27	0			
Cor Total	7.671435	53				
Std. Dev.	0.052671		R-Squared	0.987343		
Mean	0.478588		Adj R-Squared	0.980833		
C.V. %	11.00553		Pred R-Squared	0.969871		
PRESS	0.231134		Adeq Precision	37.49812		

This fact was also confirmed from the predicted vs. observed values plot for the overflow velocity in Fig. 6. The Pred R^2 was 96.99%, implying that it could explain variability in predicting new observations. This was in a reasonable agreement with the Adj R^2 of 98.08%. Adeq precision shows the signal to noise ratio; a ratio of greater than 4 is a desirable value [40]. In this investigation, the ratio was 47.50 (Table 5), indicating an adequate signal. The model can be used to navigate the design space. In case of overflow rate, a similar model description can also be presented, as seen from the model precision parameters listed in Table 6 and the normal probability and prediction plots shown in Fig.s 7 and 8, respectively.

3.3. Model construction for overflow cut-size

Introducing the equations of motion for individual particles moving through a fluid is usually complicated and simplifications have to be considered. There are many factors affecting the motion equations including particles frequency, size, shape, density, hydrophobicity, roughness, and fluid characteristics such as viscosity, motion direction, etc. Therefore, it is commonly preferred to construct such equations by estimation of all fluid forces acting on the particle, and equating them to the total fluid force. Therefore, several models have been developed to simulate two phase flows of fluid-solid systems. However, there is a general rule governing all modeling approaches that carrying the

capacity of fluid that is increased by fluid flowrate; in other word, as the fluid velocity increases, the coarser particles are carried with the fluid. In this study, the variation of classifier cut-size values against the measured overflow rates was plotted, and the best fitted equation was determined for prediction of the cut-size values at experimental levels (Table 3). The cut-size vs. overflow rate plot is shown in Fig. 9, describing that cut-size can be estimated using an exponential equation as follows,

$$d_{50} = 326.27 \times Q_o^{0.3919} \quad (20)$$

Since the modeling process is based on CFD approach which uses the overflow velocity as the process response, the measured cut-sizes were plotted vs. overflow velocity values calculated by Eq. (16) (Fig. 10) and the prediction equation was determined as follows,

$$d_{50} = 244.24 \times V_o^{0.3919} \quad (21)$$

Table 7. Analysis of variance (ANOVA) of the full factorial model to predict overflow rate.

Source	Sum of Squares	df	Mean Square	F Value	p-value Prob > F	
Model	1.727677	18	0.095982	151.6797	< 0.0001	**significant**
Feed flowrate (Q)	1.674197	2	0.837098	1322.86	< 0.0001	
Solid content (X)	0.008528	2	0.004264	6.738341	0.0033	
Baffle length (L)	0.011119	2	0.00556	8.785917	0.0008	
QX	0.009724	4	0.002431	3.841709	0.0109	
QL	0.009417	4	0.002354	3.720237	0.0126	
XL	0.014692	4	0.003673	5.804605	0.0011	
Residual	0.022148	35	0.000633			
Lack of Fit	0.022148	8	0.002768			
Pure Error	0	27	0			
Cor Total	1.749825	53				
Std. Dev.	0.025155		R-Squared	0.987343		
Mean	0.228571		Adj R-Squared	0.980833		
C.V. %	11.00552		Pred R-Squared	0.969871		
PRESS	0.052721		Adeq Precision	37.49814		

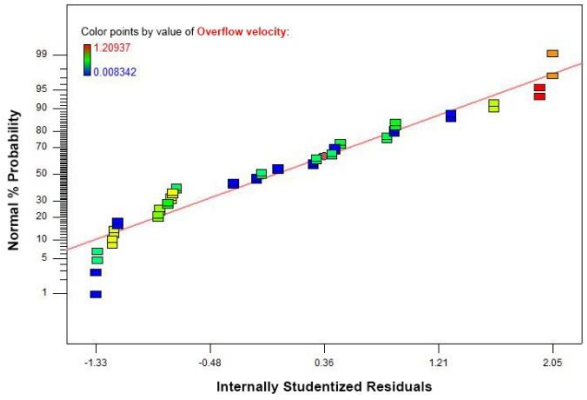

Fig. 5. Normal probability plot of the residuals for overflow velocity model.

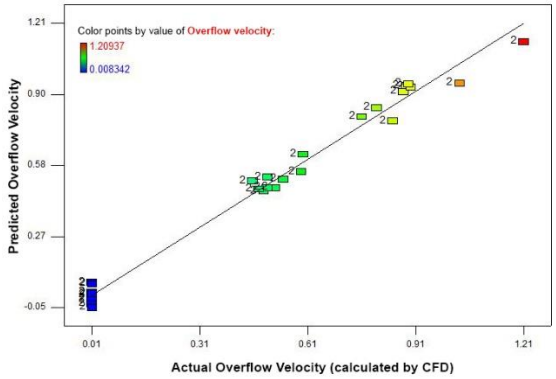

Fig. 6. Relation between observed and predicted overflow velocity values.

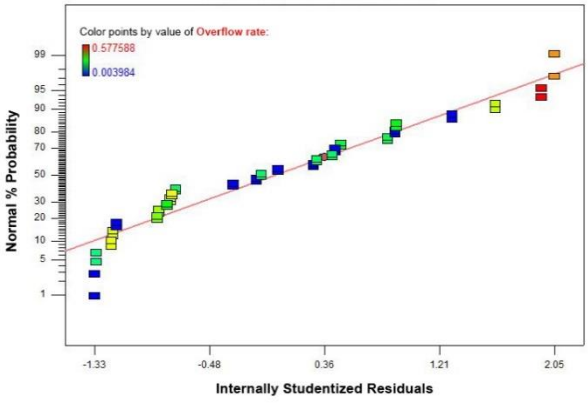

Fig. 7. Normal probability plot of the residuals for overflow rate model.

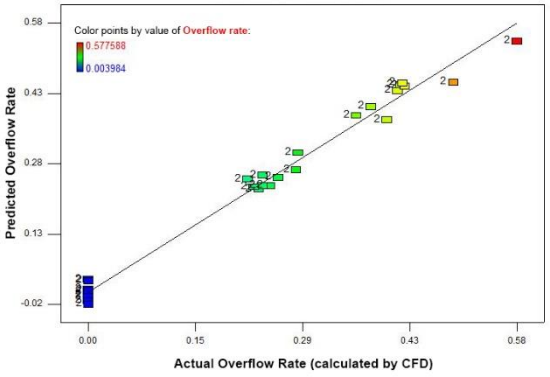

Fig. 8. Relation between observed and predicted overflow rate values.

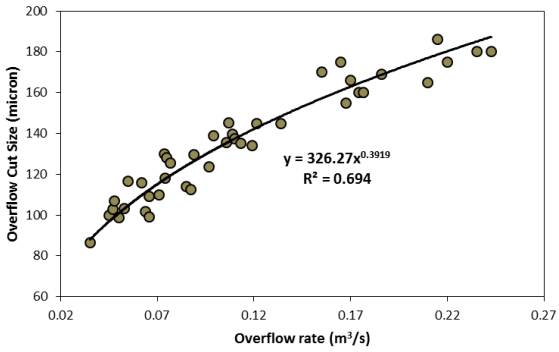

Fig. 9. Variation of measured cut-size vs. measured overflow rate.

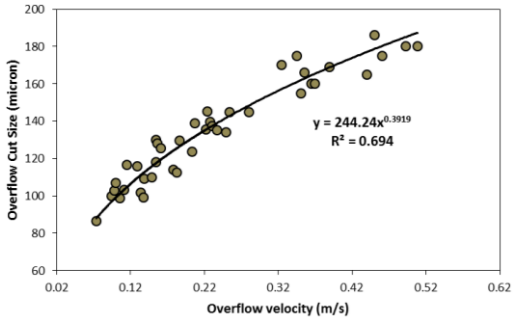

Fig. 10. Variation of measured cut-size vs. calculated overflow velocity.

Eq. (21) was used for calculation of cut-size of experimentally designed conditions and the results are shown in Table 3. Now, a prediction model for estimation of product cut-size can be developed based on the studied operating parameters by nonlinear regression procedure. The best fitted model equation proposed by DX7 software is as follows:

$$\begin{aligned}\text{Cut-size} = {} & 153.93 - 115.4Q_1 + 34.5Q_2 \\ & - 2.86X_1 - X_2 - 3.17L_1 - 1.91L_2 \\ & + 2.8Q_1X_1 + 1.9Q_2X_1 + Q_1X_2 \\ & - 1.92Q_2X_2 + 2.12Q_1L_1 + 1.46Q_2L_1 \\ & + 1.29Q_1L_2 - 1.38Q_2L_2 + 0.65X_1L_1 \\ & + 0.23X_2L_1 - 2.08X_1L_2 + 5.94X_2L_2\end{aligned} \quad (22)$$

The significance of model Eq. (22) was tested by ANOVA as given in Table 8. ANOVA results suggested that the proposed model is highly significant with a high F model of 729.96 and a very low probability p-value. Table 8 reveals that all effects, except the solid content and baffle length interaction, are the significant terms for product cut-size model. Normal probability of the residuals for product cut-size is shown in Fig. 11. As seen, almost no serious violation of the assumptions underlies the analyses that confirmed the normality assumptions and independence of the residuals. A high value of determination coefficient (R^2 = 99.73%) and adjusted correlation coefficient (Adj R^2 = 99.60%) show high significance of the model. The predicted versus observed values for cut-size plotted in Fig. 12 confirms the significance of cut-size model.

Table 8. Analysis of variance (ANOVA) of the full factorial model to predict product cut-size.

Source	Sum of Squares	df	Mean Square	F Value	p-value Prob > F	
Model	381457.1	18	21192.06	729.9627	< 0.0001	**significant**
Feed flowrate (Q)	378913	2	189456.5	6525.849	< 0.0001	
Solid content (X)	433.6728	2	216.8364	7.468953	0.0020	
Baffle length (L)	709.845	2	354.9225	12.22534	< 0.0001	
QX	407.6702	4	101.9175	3.51056	0.0164	
QL	282.5065	4	70.62663	2.432742	0.0657	
XL	710.375	4	177.5938	6.117236	0.0008	
Residual	1016.11	35	29.0317			
Lack of Fit	1016.11	8	127.0137			
Pure Error	0	27	0			
Cor Total	382473.2	53				
Std. Dev.	5.388107		R-Squared	0.997343		
Mean	153.9347		Adj R-Squared	0.995977		
C.V. %	3.500255		Pred R-Squared	0.993676		
PRESS	2418.755		Adeq Precision	69.39023		

3.4. Analysis of main effects

The effects of operating parameters on overflow cut-size values were analysed based on overflow velocity. These effects were modelled by Eqs. (18) and (22), and were applied to interpret the main effects in combination with CFD graphical results. Fig. 13 shows the effect of feed pulp solid content on the overflow velocity and cut-size. Due to the effect of hindered-settling condition, as the solid content increases, the cut size increases as well. Generally, classifiers use two settling mechanisms, free settling to increase the influence of particle size on the classification and hindered-settling to increase the effect of particle density on separation. Free settling refers to the conditions under which the particles sink in a classification chamber that contains a fluid of a volume significantly larger than that of the particles; thus, particle crowding can be considered negligible. For well-dispersed ore pulps, free settling is predominant when the mass content of solids is less than 15%. As the pulp solid percentage increases, the effect of particle crowding becomes more apparent and the settling rate of the particles decreases and the pulp behaves as a heavy media which its density is equal to the pulp, not the carrier water; therefore, hindered-settling conditions become dominant. Due to high density and viscosity of the pulp under hindered settling conditions, the resistance to the particles that fall down in the classification chamber is mainly caused by the turbulence regime, and consequently, the cut size value increases [6]. Fig. 13 also shows that the effect of solid content is fairly significant due to the light turbulence conditions in classifier chamber as seen in CFD patterns.

This effect was also predicted by statistical analyses. As seen in Tables 5 and 7, the *p*-values for both the overflow velocity (Table 6) and the cut-size (Table 8) are higher than that of the other parameters.

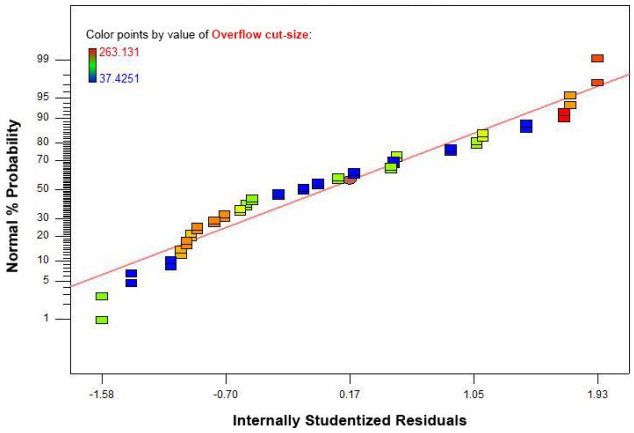

Fig. 11. Normal probability plot of the residuals for overflow cut-size model.

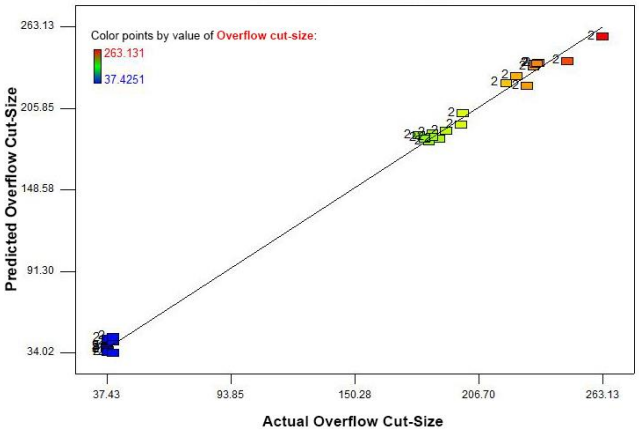

Fig. 12. Relation between observed and predicted overflow cut-size values.

Fig. 14 shows the main effect plots for cut-size and overflow velocity vs. feed pulp flowrate. As the feed flowrate increases, the overflow velocity, and consequently the product cut-size directly increase. In general, two reasons can be attributed to the increased cut-size value by feed flowrate; as shown in CFD simulated fluid velocity patterns inside the classifier chamber, the turbulent regime inside the classifier sorting column increases through increasing the feed flow rate, and therefore, the free-settling separation condition approaches to the hindered-settling mechanism. Under hindered-settling conditions, inter-particle collisions prevent coarse particles to freely settle downward the underflow outlet. Moreover, particles retention time also decreases with increasing of flowrate, so preventing the effective separation of particles.

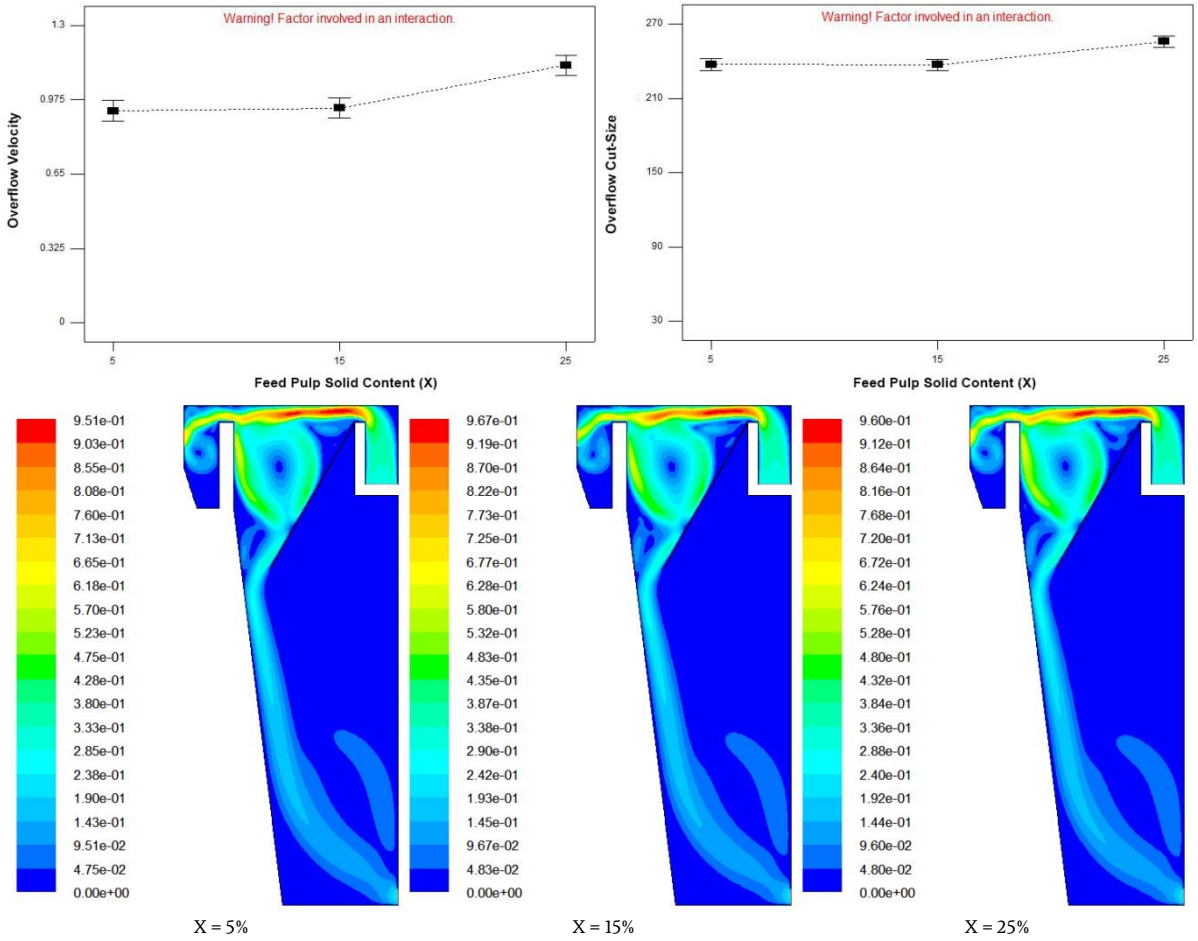

Fig. 13. Effect of feed pulp solid content on overflow velocity and cut-size.

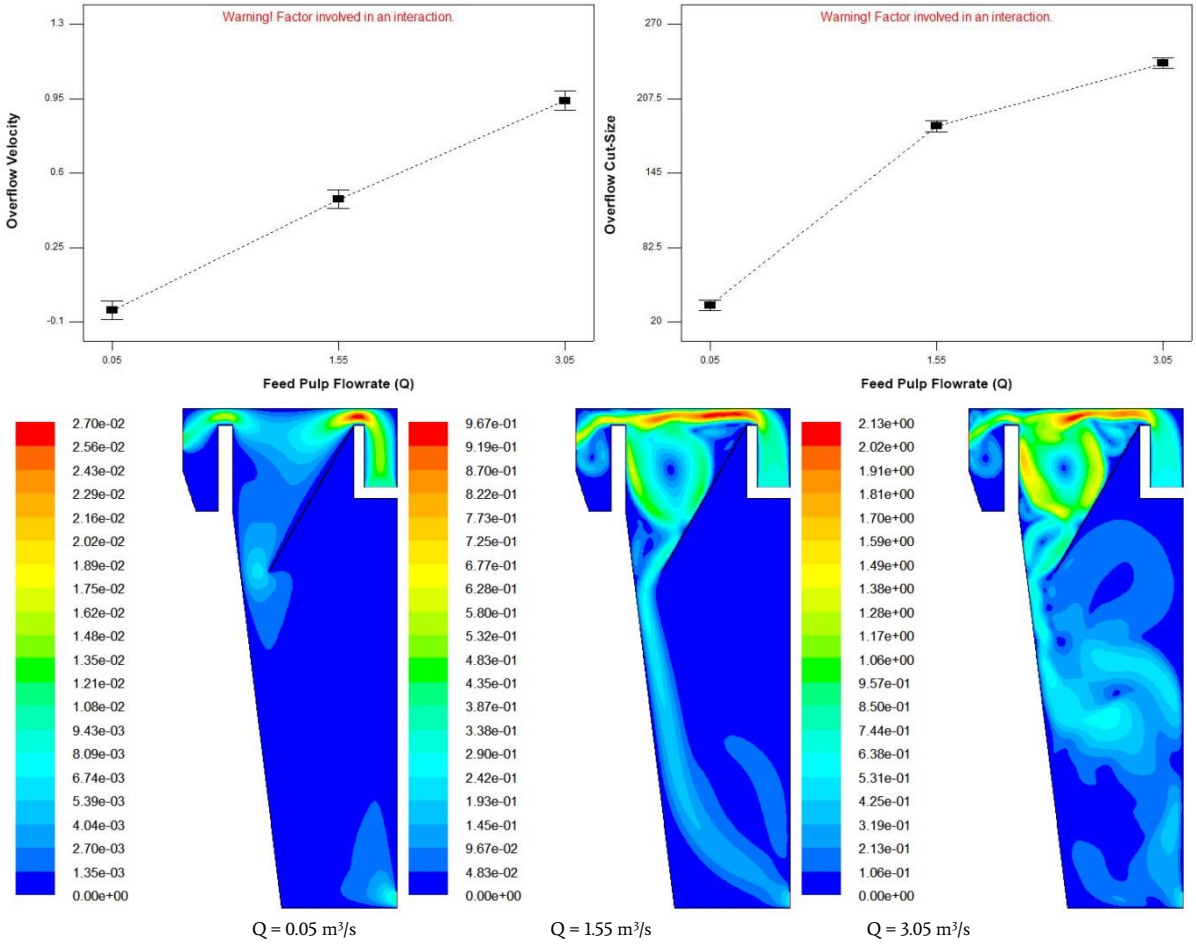

Fig. 14. Effect of feed pulp flowrate on overflow velocity and cut-size.

The effect of baffle length on overflow responses is shown in Fig. 15. Baffle length has a fair but negative effect on the overflow velocity and cut-size. Fluid velocity patterns inside the classifier simulated for different baffle lengths are also shown in Fig. 15. As seen, the turbulency inside the column decreases as the baffle length is increased. These patterns clearly show the positive action of baffle to control the turbulent environment. Baffle decreases the turbulency by breaking and dispersing the pulp stream lines. Long baffle plate decreases the overflow velocity and product cut-size by moderating the turbulence regime into the sorting chamber.

3.5. Analysis of interaction effects

The three-dimensional (3D) plots of the model response vs. two independent variables varying within their experimental levels while maintaining other variables are at their mid-levels can give useful information about their relationships [48]. Therefore, in order to gain better understanding of individual effects of the studied operating variables and their corresponding interaction effects on other variables, the 3D plots of the overflow responses were provided based on the nonlinear models proposed by DX7 software. Since the models in this study had three independent variables, only one variable was kept constant at its mid-level for each plot. The influence of the studied operating variables on the overflow velocity and cut-size is visualized in Fig.s 16 and 17. As seen, plots for both responses show similar patterns. It should be noted that analyzing the effects based only on the shape of the plots is not true and ANOVA results are also necessary for interpreting the interaction effects. Referring to ANOVA tables, it can be found that all interaction effects on the overflow velocity are significant (Table 6) whereas in case of the overflow cut-size, the interaction between feed flowrate and baffle length is not high enough to be considered significant (p value > 0.05; Table 8); thus, it can be neglected. As shown in the main effect plots, the feed flowrate and solid content had positive effects on the overflow velocity and cut-size. Therefore, it is expected that the interactions follow a similar trend. Fig.s 16 and 17 show that the overflow responses increase by simultaneously increasing of the feed flowrate and solid content. The response plot of feed flowrate and baffle length indicates that the responses increase by feed flowrate in presence and absence of baffle plate; this means that the effect of feed flowrate is superior to baffle effect. However, at constant feed flowrates, a nonlinear trend is observed for baffle length effect, as seen for the solid content effect in feed flowrate and solid content response plot. This trend may be attributed to the interaction effect of solid content and baffle length. It was shown in main effect plots in which the overflow responses decreased as the length of baffle plate was increased. However, Fig.s 16 and 17 show a slight increase of overflow responses when feed solid content exceeds about 20%. At high solid content, these conditions are rarely observed in practice, as claimed by technical engineers, and hindered-settling condition becomes the dominant effect especially in classifier equipped by a full length baffle. When the solid content increases, the long baffle prevents the continuous swarm of particles to freely flow inside the column. Therefore, stream lines concentrate above the baffle plate and are directed to the overflow outlet. This will increase the velocity of overflow. Therefore, it can be concluded that baffle plays its positive role under free-settling condition which is initially considered in original layout of Zarand Coal Washing Plant, i.e. an operating solid content of about 15%.

22

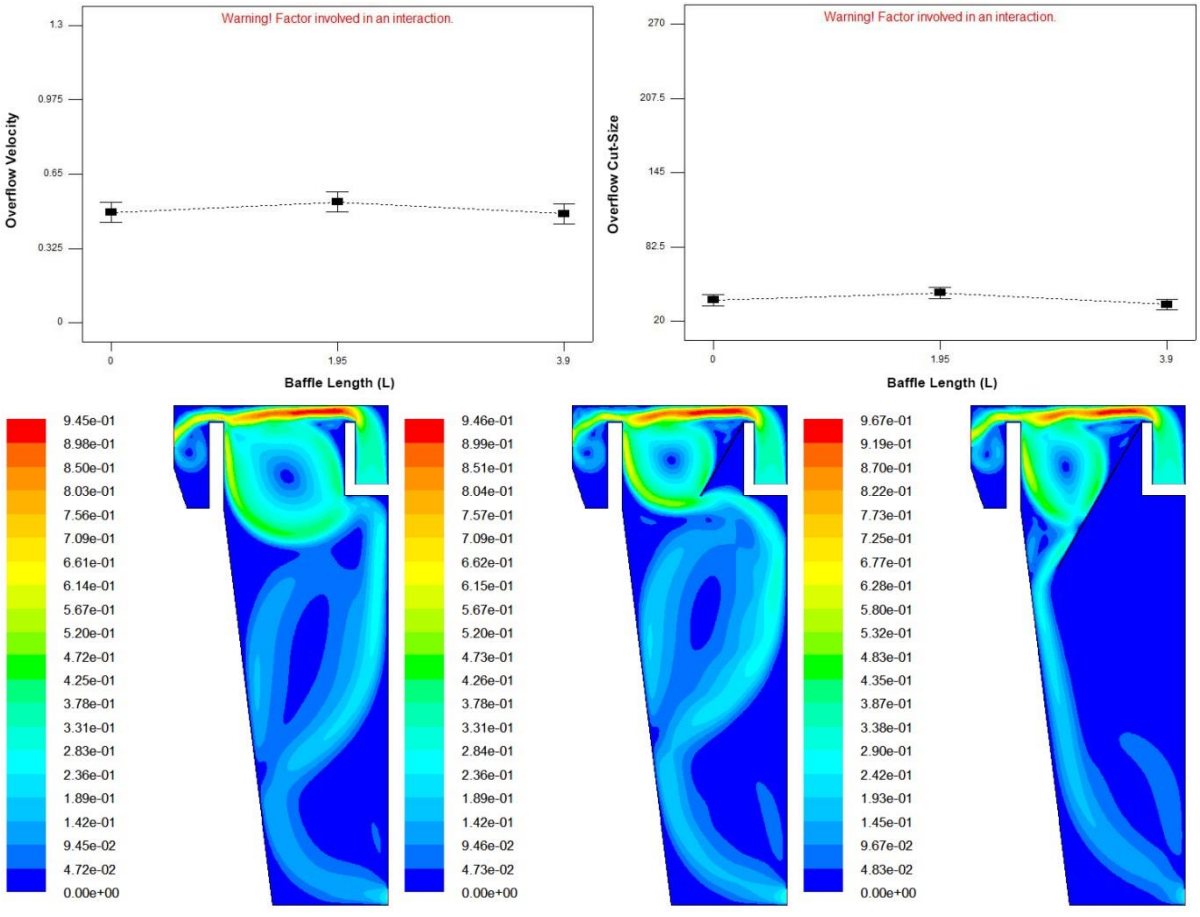

L = baffle removed L = 1.95 m L = 3.9 m

Fig. 15. Effect of baffle length on overflow velocity and cut-size.

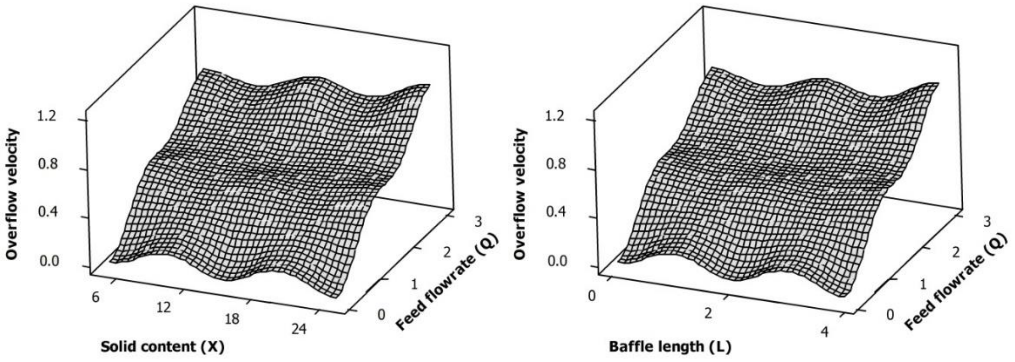

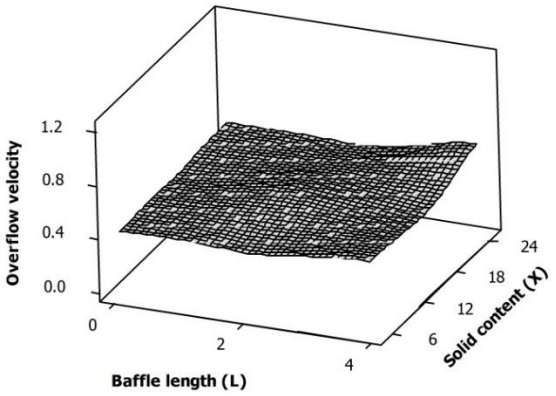

Fig. 16. The response plot showing the effects of operating variable on overflow velocity.

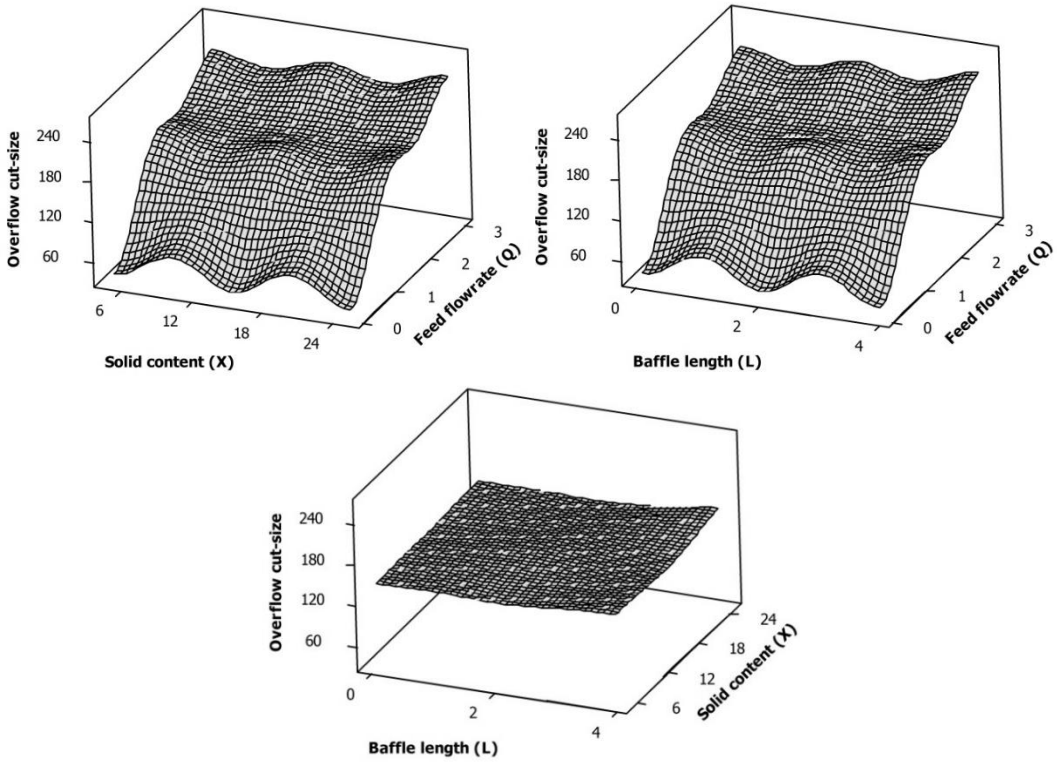

Fig. 17. The response plot showing the effects of operating variable on overflow cut-size.

4. Conclusions

Today, computational fluid dynamics and experiments design are known as two analyses tools that engineers can apply them for experimental interpretation and process optimization. Each method has its own advantages and limitations. A CFD-DOE combined modeling method was developed in present study to provide the condition in which engineers can benefit from the advantages of both modeling methods. The method consists of two general steps: numerical prediction of process response values using CFD method, and development of a statistical parametric model to predict the practical response values under real industrial conditions. Validation of suggested method was also confirmed by hydrodynamic simulation of an industrial hydraulic classifier in Zarand Coal Washing Plant (Zarand, Iran). Prediction of the overflow cut-size of studied classifier, as the process response, was carried out using the parametric model developed by the proposed model. The model equation provided a fitting agreement of about 70% between the predicted and experimentally measured cut-size values. This relatively low but acceptable modeling precision can mainly be attributed to the industrial target system simulated in this study. It is well known that the coal processing systems are usually involved with difficulties when they are parametrically simulated. This is due to the extremely varying properties of coal feed into the system. Therefore, validation of proposed modeling method using the obtained data from a non-coal system may lead to more precise results. In addition, CFD modeling in this paper is conducted using predefined functions available in Fluent software, and no extra codes were generated for modeling. Thus, it is expected that more reliable results are obtained by developing specified coded to the studied system. Although further studies are required to fully understand the benefits and applicability of the proposed modelling method, it seems to be a useful and promising tool to simulate every type of devices that work based on fluid flows.

Acknowledgment

Technical supports from the Zarand Coal Washing Plant (Zarand, Iran) and INVENTIVE® Mineral Processing Research Center (Zarand, Iran) are acknowledged.

REFRENCES

[1] Priester, M., Hentschel, T., & Benthin, B. (1993). Tools for Mining: Techniques and Processes for Small Scale Mining, Friedr. Vieweg & Sohn Verlagsgesellschaft GmbH, Munich.

[2] Sarrafi, A.R. (1987). Mineral Separation Device Supported by Hydrocyclone Mechanism with Closed Circuit, Industrial and scientific research organization, Kerman.

[3] Kelly, E.G., & Spottiswood, D.J. (1989). Introduction to Mineral Processing, John Wiley & Sons, Queens Land.

[4] Vijayendra, H.G. (1995). Handbook of Mineral Processing, New Delhi Publication, New Delhi.

[5] Taggart, A.F. (1945). Handbook of Mineral Dressing, John Willey & Sons, New York.

[6] Wills, B.A., & Finch, J.A. (2016). Mineral Processing Technology, 8th ed.,Elsevier Science and Technology, Amsterdam.

[7] Park, H. (2015). CFD Advantages and Practical Applications, Glumac, Seattle.

[8] Bhaskar, K.U., Murthy, Y.R., Raju, M.R., Tiwari, S., Srivastava, J.K., & Ramakrishnan, N. (2007). CFD simulation and experimental validation studies on hydrocyclone. Miner. Eng., 20, 60–71.

[9] Bhaskar, K.U., Murthy, Y.R., Ramakrishnan, N., Srivastava, J.K., Sarkar, S., & Kumar, V. (2007). CFD validation for flyash particle classification in hydrocyclones. Miner. Eng., 20(3), 290–302.

[10] Narasimha, M., Brennan, M.S., & Holtham, P.N. (2012). CFD modeling of hydrocyclones: prediction of particle size segregation. Miner. Eng., 39, 173–183.

[11] Swain, S., & Mohanty, S. (2013). A 3-dimensional Eulerian–Eulerian CFD simulation of a hydrocyclone. Appl. Math. Modell., 37(5), 2921–2932.

[12] Kępa, A. (2013). The efficiency improvement of a large-diameter cyclone–The CFD calculations. Sep. Purif. Technol., 118, 105–111.

[13] Safa, R., & Goharrizi, A.S. (2014). CFD simulation of an industrial hydrocyclone with Eulerian–Eulerian approach: A case study. Int. J. Mining Sci. Technol., 24(5), 643–648.

[14] Johansson, R., & Evertsson, M. (2014). CFD simulation of a centrifugal air classifier used in the aggregate industry. Miner. Eng., 63, 149–156.

[15] Johansson, R., & Evertsson, M. (2012). CFD simulation of a gravitational air classifier. Miner. Eng., 33, 20–26.

[16] Jarkani, S.A., Khoshdast, H., Sam, A., & Shariat, E. (2014). Modeling the effects of mechanical parameters on the hydrodynamic behavior of vertical current classifiers. Int. J. Mining Sci. Technol., 24(1), 123–127.

[17] Bhardwaj, O.P., Bandyopadhyay, A., & Rao, T.C. (1987). Plant performance studies on a hydraulic cone classifier as a secondary classifier. Int. J. Miner. Process., 21, 217–223.

[18] Klumpar, I.V. (1992). Measuring and optimizing air classifier performance. Sep. Technol., 2, 124–135.

[19] Heiskanen, K.G.H. (1996). Developments in wet classifiers. Int. J. Miner. Process., 44–45, 29–42.

[20] Honaker, R.Q., & Mondal, K. (2000). Dynamic modeling of fine coal separations in a hindered- bed classifier. Int. J. Coal Prep. Util., 21, 211–232.

[21] Vakamalla, T.R., Koruprolu, V.B., Arugonda, R., & Mangadoddy, N. (2017). Development of novel hydrocyclone designs for improved fines classification using multiphase CFD model. Sep. Purif. Technol., 175, 481–497.

[22] Galvin, K.P., Callen, A., Zhou, J., & Doroodchi, E. (2005). Performance of the reflux classifier for gravity separation at full scale. Miner. Eng., 18, 19–24.

[23] Zhou, J., Walton, K., Laskovski, D., Duncan, P., & Galvin, K.P. (2006). Enhanced separation of mineral sands using the reflux classifier. Miner. Eng., 19, 1573–1579.

[24] Feng, Y., Liu, J., & Liu, S. (2008). Effects of operating parameters on flow field in a turbo air classifier. Miner. Eng., 21, 598–604.

[25] Galvin, K.P., Callen, A.M., & Spear, S. (2010). Gravity separation of coarse particles using the reflux classifier. Miner. Eng., 23(4), 339–349.

[26] Zhang, L., Liu, W., & Zhang, Y. (2016). Calculation of teeter bed height of teetered bed separator based on jet theory. Powder Technol., 295, 225–233.

[27] Tripathy, S.K., Mallick, M.K., Singh, V., & Murthy, Y.R. (2013). Preliminary studies on teeter bed separator for separation of manganese fines. Powder Technol., 239, 284–289.

[28] Maharaj, L., Pocock, J., & Loveday, B.K. (2007). The effect of distributor configuration on the hydrodynamics of the teetered bed separator. Miner. Eng., 20(11), 1089–1098.

[29] Amariei, D., Michaud, D., Paquet, G., & Lindsay, M. (2014). The use of a reflux classifier for iron ores: Assessment of fine particles recovery at pilot scale. Miner. Eng., 62, 66–73.

[30] Campbell, Q. P., le Roux, M., & Smith, I.G.T. (2015). Water-only laboratory coal fractionation using the reflux classifier. Miner. Eng., 83, 59–63.

[31] Galvin, K.P., Zhou, J., Price, A.J., Agrwal, P., & Iveson, S.M. (2016). Single-stage recovery and concentration of mineral sands using a reflux™ classifier. Miner. Eng., 93, 32–40

[32] Khoshdast, H., Khoshdast, H., Shojaei, V. (2014). Effect of baffle design parameters on fluid dynamic response of a coal classifier. J. Mining World Express, 3(1), 15–23.

[33] Geiger, F., Velten, K., Methner, F-J. (2012). 3D CFD simulation of bottle emptying processes. J. Food Eng., 109(3), 609–618.

[34] Krastev, V.K., Falcucci, G., Jannelli, E., Minutillo, M., & Cozzolino, R. (2014). 3D CFD modeling and experimental characterization of HT PEM fuel cells at different anode gas compositions. Int. J. Hydrogen Energ., 39(36), 21663–21672.

[35] Tabatabaeikia, S., Ghazali, N.N.B.N., Chong, W.T., Shahizare, B., Izadyar, N., Esmaeilzadeh, A., & Fazlizan, A. (2016). Computational and experimental optimization of the exhaust air energy recovery wind turbine generator. Energ. Convers. Manage., 126, 862–874.

[36] Alalm, M.G., Nasr, M., & Ookawara, S. (2016). Assessment of a novel spiral hydraulic flocculation/sedimentation system by CFD simulation, fuzzy inference system, and response surface methodology. Sep. Purif. Technol., 169, 137–150.

[37] Yang, M., Yu, D., Liu, M., Zheng, L., Zheng, X., Wei, Y., Wang, F., & Fan, Y. (2017). Optimization of MBR hydrodynamics for cake layer fouling control through CFD simulation and RSM design. Bioresource Technol., 227, 102–111.

[38] Obeng, D.P., Morrell, S., & Napier-Munn, T.J. (2005). Application of central composite rotatable design to modeling the effect of some operating variables on the performance of the three-product cyclone. Int. J. Miner. Process., 76(3), 181–92.

[39] Aghajani, S.A., Soltani, G.A., Ebrahimzadeh, G.M., Sarafi, A., Razmirad, M., & Abdollahi, H. (2013). Application of response surface methodology and central composite rotatable design for modeling the influence of some operating variables of the lab scale thickener performance. Int. J. Mining Sci. Technol., 23, 717–724.

[40] Montgomery, D.C. (2001). Design and Analysis of Experiments, John Wiley & Sons, New York.

[41] Dehghani-Sanij M.A. (2008). Numerical simulation with Fluent 6.3 Software, Naghoos-e Andisheh Publisher, Tehran.

[42] Golshahifar M. (2009). Practical Fluent, Sanei Shahmirzadi

Publication, Tehran.

[43] Razavi Parizi, S.E. (2010). Introduction to Linear Regression Analysis, Shahid Bahonar University Press, Kerman.

[44] Al-Shemmeri, T. (2012). Engineering Fluid Mechanics, Ventus Publishing ApS, Denmark.

[45] Cornell, J.A. (1990). How to Apply Response Surface Methodology, American society for quality control, Wisconsin.

[46] Clarke, G.M., & Kempson, R.E. (1997). Introduction to the Design and Analysis of Experiments, Arnold, London.

[47] Yetilmezsoy, K., Demirel, S., & Vanderbei, R.J. (2009). Response surface modeling of Pb(II) removal from aqueous solution by Pistacia vera L.: Box–Behnken experimental design. J. Hazard. Mater., 171, 551–562.

[48] Liu, H.L., & Chiou, Y.R. (2005). Optimal decolorization efficiency of Reactive Red 239 by UV/TiO_2 photocatalytic process coupled with response surface methodology. Chem. Eng. J., 112, 173–179.